Stereochemically Nonrigid Seven-Coordinate Molecules. A Detailed Mechanistic Analysis for the Molecule $CrH_2[P(OCH_3)_3]_5$†,‡

Frederic A. Van-Catledge, Steven D. Ittel,* and J. Peter Jesson

Central Research & Development Department, E. I. du Pont de Nemours & Company, Experimental Station, Wilmington, Delaware 19898

Received June 28, 1984

$Cr[P(OMe)_3]_6$, prepared by the cocondensation of Cr atoms and $P(OMe)_3$, reacts with hydrogen to give $Cr[P(OMe)_3]_5H_2$, a molecule which is fluxional on the NMR time scale. The ^1H and $^{31}P\{^1H\}$ NMR line-shape changes for the complex $AB_2CC'XX'$ spin system have been analyzed in complete form over a temperature range encompassing slow- and fast-exchange limits. The distinguishable basic sets of permutations were determined by abstract mechanistic analysis in terms of the point group of the molecule and the possible nuclear permutations. The observed line shapes were then compared with line shapes calculated for each of the sets. Two of the 16 possible basic sets gave simulated line shapes in reasonable agreement with experiment. The two sets correspond to identical phosphorus permutational behavior and differ only in the question of whether the two hydrogens permute or not. The case in which the hydrogens do not permute is marginally preferred in terms of closeness of fit to the experimental spectra. On the basis of the distorted pentagonal-bipyramidal geometry established for the molecule, possible physical mechanisms corresponding to the allowed permutations are considered. It is concluded that the most probable mechanism is closely related to the Berry process in five-coordinate complexes.

Introduction

We have reported the synthesis[1a] of $CrH_2[P(OCH_3)_3]_5$, A, an interesting, seven-coordinate molecule which is fluxional on the NMR time scale.[1b] All seven atoms coordinated to the central metal are magnetically active, allowing a detailed mechanistic study. Several additional MH_2L_5 systems have been reported,[2] but none are amenable to the type of NMR investigation detailed here. In contrast to earlier work on six-coordinate MH_2L_4 systems,[3] which were expected to be stereochemically rigid, fluxional behavior in the seven-coordinate MH_2L_5 species was anticipated; nonrigidity is a common phenomenon in seven coordination.[4] Major interest, therefore, lies in slowing the exchange process on the NMR time scale and extracting mechanistic information in addition to the more readily available kinetic information.

The mechanisms of ligand exchange in seven coordination are poorly understood. Mechanistic information has been obtained for systems containing chelating ligands;[4a,k,r-u] these were complicated by the presence of more than one isomer or the possibility of "arm-off" mechanisms. More importantly, the multidentate character of the ligands restricts the mechanistic possibilities, and, therefore, these systems do not relate as clearly to the fundamental questions of seven-coordinate stereochemistry.

Experimental Section

All manipulations were carried out in a dry nitrogen atmosphere. Solvents were dried by standard techniques. The metal vapor synthesis technique[5] was used to prepare $Cr[P(OMe)_3]_6$ which was reacted with hydrogen to yield $Cr[P(OMe)_3]_5H_2$. Details are presented elsewhere.[6]

NMR spectra were collected in the FT mode on a Bruker HFX-90 spectrometer equipped with a Digilab FTS/NMR-3 data system and pulser. The NMR samples were dissolved in $CHClF_2$ under a nitrogen atmosphere. $^{31}P\{^1H\}$ spectra (36.43 MHz) were run in 10-mm tubes, with fluorine field-frequency stabilization using the fluorine signal of the solvent. ^1H spectra were run in 5-mm tubes, a small amount of CD_2Cl_2 being added as an internal deuterium lock. The dynamic range problem introduced by the solvent signal in the ^1H spectra was diminished in the following

† This paper is dedicated to the memory of Earl Muetterties in recognition of his many contributions to inorganic and organometallic chemistry.

‡ Contribution No. 2763.

(1) (a) Ittel, S. D.; Tolman, C. A. U.S. 4 155 925, May 22, 1979. (b) Van-Catledge, F. A.; Ittel, S. D.; Tolman, C. A.; Jesson, J. P. *J. Chem. Soc., Chem. Commun.* **1980**, 254.

(2) (a) Jones, R. A.; Wilkinson, G.; Galas, A. M. R.; Hursthouse, M. B. *J. Chem. Soc., Chem. Commun.* **1979**, 926. (b) Choi, H. W.; Gavin, R. M.; Muetterties, E. L. *Ibid.* **1979**, 1085. (c) Choi, H. W.; Muetterties, E. L. *J. Am. Chem. Soc.* **1982**, *104*, 153. (d) Hursthouse, M. B.; Lyons, D.; Thornton-Pett, M.; Wilkinson, G. *J. Chem. Soc., Chem. Commun.* **1983**, 476. (e) Chiu, K. W.; Jones, R. A.; Wilkinson, G.; Galas, A. M. R.; Hursthouse, M. B.; Malik, K. M. A.; *J. Chem. Soc., Dalton Trans.* **1981**, 1204. (f) Lyons, D.; Wilkinson, G.; Thornton-Pett, M.; Hursthouse, M. B. *Ibid.* **1984**, 695. (g) Kubas, G. J. *J. Chem. Soc., Chem. Commun.* **1980**, 61. (h) Vergamini, P. J.; Kubas, G. J.; Ryan, R. D.; Wasserman, H. J.; Larson, A. C. "Program, ACA Meeting", Mar, 1983, Series 2, Vol. 11, No. 1, Abstract J5. (i) Kubas, G. J.; Ryan, R. R.; Swanson, B. I.; Vergamini, P. J.; Wasserman, H. J. *J. Am. Chem. Soc.* **1984**, *106*, 451.

(3) Meakin, P.; Muetterties, E. L.; Tebbe, F. N.; Jesson, J. P. *J. Am. Chem. Soc.* **1971**, *93*, 4701.

(4) (a) Muetterties, E. L.; Packer, K. J. *J. Am. Chem. Soc.* **1964**, *86*, 293. (b) Gillespie, R. J.; Quail, J. W. *Can. J. Chem.* **1964**, *42*, 2671. (c) Malatesta, L.; Freni, M.; Valenti, V. *Gazz. Chim. Ital.* **1964**, *94*, 1278. (d) Pinnavaia, T. J.; Fay, R. C. *Inorg. Chem.* **1968**, *7*, 502. (e) Johnson, B. F. G.; Al-Obaidi, K. H.; McCleverty, J. A. *J. Chem. Soc. A* **1969**, 1668. (f) Elder, M.; Evans, J. G.; Graham, W. A. G. *J. Am. Chem. Soc.* **1969**, *91*, 1245. (g) Howe, J. J.; Pinnavaia, T. J. *Ibid.* **1970**, *92*, 7342. (h) Davis, R.; Hill, M. N. S.; Holloway, C. E.; Johnson, B. F. G.; Al-Obaidi, K. H. *J. Chem. Soc. A* **1971**, 994. (i) Ginsberg, A. P.; Tulley, M. E. *J. Am. Chem. Soc.* **1973**, *95*, 4750. (j) Bhat, A. N.; Fay, R. C.; Lewis, D. F.; Lindmark, A. F.; Strauss, S. H. *Inorg. Chem.* **1974**, *12*, 886. (k) Meakin, P.; Guggenberger, L. J.; Tebbe, F. N.; Jesson, J. P. *Ibid.* **1974**, *13*, 1025. (l) Pinnavaia, T. J.; Howe, J. J.; Teets, R. G. *Ibid.* **1974**, *13*, 1074. (m) Schrock, R. R.; Meakin, P. *J. Am. Chem. Soc.* **1974**, *96*, 5288. (n) Chatt, J.; Dilworth, J. R. *J. Chem. Soc., Chem. Commun.* **1974**, 508. (o) Henrick, K.; Wild, S. B. *J. Chem. Soc., Dalton Trans.* **1974**, 2500. (p) Given, K. W.; Matson, B. M.; Pignolet, L. H. *Inorg. Chem.* **1976**, *15*, 3152. (q) Cullen, W. R.; Mihichuk, L. M. *Can. J. Chem.* **1976**, *54*, 2548. (r) Albright, J. O.; Brown, L. D.; Datta, S.; Kouba, J. K.; Wreford, S. S.; Foxman, B. M. *J. Am. Chem. Soc.* **1977**, *99*, 5518. (s) Domaille, P. J.; Harlow, R. L.; Wreford, S. S. *Organometallics* **1982**, *1*, 935. (t) Albright, J. O.; Datta, S.; Dezube, B.; Kouba, J. K.; Marynick, D. S.; Wreford, S. S.; Foxman, B. M. *J. Am. Chem. Soc.* **1979**, *101*, 611. (u) Templeton, J. L.; Ward, B. C. *J. Am. Chem. Soc.* **1981**, *103*, 3743. (v) Templeton, J. L.; Ward, B. C. *Inorg. Chem.* **1980**, *20*, 1753. (w) Wreford, S. S.; Kouba, J. K.; Kirner, J. F.; Muetterties, E. L.; Tavanalepour, I.; Day, V. W. *J. Am. Chem. Soc.* **1980**, *102*, 1558. (x) Reger, D. L; Swift, C. A.; Lebioda, L. *Inorg. Chem.* **1984**, *23*, 349. (y) Siedle, A. R.; Newmark, R. A.; Pignolet, L. H.; Howells, R. D. *J. Am. Chem. Soc.* **1984**, *106*, 1510.

(5) (a) Ittel, S. D.; Van-Catledge, F. A.; Jesson, J. P. *J. Am. Chem. Soc.* **1979**, *101*, 3874. (b) For a general introduction, see also Chapter 2: *Inorg. Synth.* **1979**, *19*, 59.

(6) Ittel, S. D.; Van-Catledge, F. A.; Tolman, C. A. *Inorg. Chem.* **1984**, *23*, 0000.

0276-7333/85/2304-0018$01.50/0

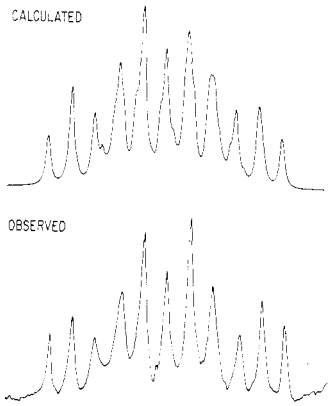

Figure 1. 90-MHz ^1H NMR spectrum of $CrH_2[P(OCH_3)_3]_5$ at −130 °C in $CHClF_2$ solution together with a simulation obtained assuming an $AB_2CC'XX'$ spin system and the NMR parameters listed in the text.

manner: The center frequency for the 90-MHz pulse was set 1 kHz upfield from Me_4Si. The free-induction-decay signal was accumulated after passing through an active bandpass filter (Krohn-Hite Model 310-C, 24 db/octave attenuation with corner frequencies set at 20 Hz and 1 kHz). The spectra obtained in this manner are reversed. (Note, however, that all figures in this paper show increasing field from left to right in the conventional manner.)

Temperatures were measured with a copper–constantan thermocouple located just below the sample tube and were calibrated by using a similar thermocouple held coaxially in a spinning sample tube containing pure solvent. ^{31}P chemical shifts are given in parts per million from external 85% H_3PO_4. Downfield shifts are taken to be positive as recommended by IUPAC. ^1H chemical shifts are relative to Me_4Si assigned as 0 ppm.

Results

Analysis of Limiting Exchange NMR Spectra for $CrH_2[P(OCH_3)_3]_5$. In view of the role that the assignment of the nuclear spin system ($AB_2CC'XX'$ for ^1H and AB_2C_2 for $^{31}P\{^1H\}$) plays in establishing the ground-state geometry of the complex, it is important to consider how the spin systems were determined and whether there are attendent uncertainties in the assignment. In the high-temperature limit, the ^{31}P and ^1H spectra correspond to a triplet and sextet, respectively, with the proper intensity distribution. The temperature-dependent behavior of the spectra was found to be independent of concentration and unaffected by added trimethyl phosphite. The effective unimolecular character and the preservation of spin correlation show that the exchange process is intramolecular.[7]

The 36.43-MHz $^{31}P\{^1H\}$ spectrum in the slow-exchange limit was first simulated as an AB_2C_2 spin system using first-order approximations. The coupling constants from this analysis provided the basis for a preliminary determination of the relative signs of the parameters J_{AB}, J_{BC}, and J_{AC}. The coupling constants were of like sign, and selected sign changes did not improve the match between calculated and experimental spectra, even with variations in magnitude.

The AC_2 subsystem was sufficiently first order to permit a direct determination of J_{AC}. An extensive set of simulations was accumulated for an $ABCD_2$ model. Within the limits of visual fitting, the best match was obtained with $\delta_B \approx \delta_C$, $J_{AB} \approx J_{AC}$, and $J_{BD} \approx J_{CD}$. After further testing, we concluded that within the limits of determination, the spin system is AB_2C_2.

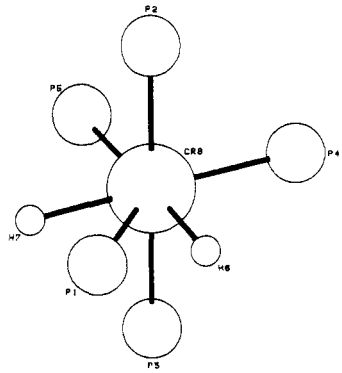

Figure 2. Structure and nuclear labeling scheme assumed for $CrH_2[P(OCH_3)_3]_5$ in the discussion sections of this paper.

To complete the analysis, the ^{31}P NMR spectrum was recorded with single frequency irradiation of the ^1H peak corresponding to the OCH_3 groups of the phosphite ligands. The A and B subsystems showed a clear triplet splitting while the C subsystem was more complex. Coupling constants for the $CC'XX'$ subsystem were estimated by a least-squares fit of the 90-MHz ^1H spectrum. The technique used a first-order model and a simplified version of the method reported by Heinzer.[8] These parameters are presumed to be accurate to ~±5 Hz. The slow exchange limit (−130 °C) 90-MHz ^1H hydride spectrum is shown in Figure 1 together with a simulation calculated assuming an $AB_2CC'XX'$ spin system with the following parameters (nuclear labeling scheme as in Figure 2 [vide infra]):

$$J_{AB} = J_{12} = J_{13} = \pm 86 \text{ Hz}$$

$$J_{AC} = J_{14} = J_{15} = \pm 32 \text{ Hz}$$

$$J_{BC} = J_{24} = J_{25} = J_{34} = J_{35} = \pm 78 \text{ Hz}$$

$$J_{AX} = J_{16} = J_{17} = \pm 81 \text{ Hz}$$

$$J_{BX} = J_{26} = J_{27} = \pm 25 \text{ Hz}$$

$$\left.\begin{matrix} J_{CX} = J_{46} = J_{57} \\ J_{CX'} = J_{47} = J_{56} \end{matrix}\right\} \approx \left\{\begin{matrix} \pm 80 \text{ Hz} \\ \pm 53 \text{ Hz} \end{matrix}\right.$$

$$J_{CC'} = J_{45} \approx \pm 8 \text{ Hz}$$

$$J_{XX'} = J_{67} \approx \mp 11 \text{ Hz}$$

$$\delta_A = \delta_1 = 222.5 \qquad \delta_C = \delta_4 = \delta_5 = 190.1$$

$$\delta_B = \delta_2 = \delta_3 = 204.6 \qquad \delta_X = \delta_6 = \delta_7 = -7.95$$

Assignment of the Effective Geometry in the Slow-Exchange Limit for $CrH_2[P(OCH_3)_3]_5$. The $AB_2CC'XX'$ assignment requires the presence of two orthogonal planes of symmetry; as a result, the point group of the molecule in the slow-exchange limit is C_{2v}. Britton and Dunitz[9] have systematically evaluated all possible nonisomorphic convex polyhedra with seven vertices. There are 34 polyhedra, only 11 of which have symmetry C_{2v} or higher for the case in which all ligands are identical. The effective solution geometry of the CrH_2P_5 framework must conform to one of these 11 polyhedra.

In Table I, each of the 11 polyhedra is considered in sequence of decreasing order of the axis of highest symmetry. The analysis is carried out in a formal manner without referring to known preferences in seven-coordinate

(7) (a) Muetterties, E. L. *Inorg. Chem.* **1965**, *4*, 769. (b) Muetterties, E. L. *J. Am. Chem. Soc.* **1968**, *90*, 5097.

(8) Heinzer, J. *J. Magn. Reson.* **1977**, *26*, 301.
(9) Britton, D.; Dunitz, J. D. *Acta Crystallogr., Sect. A* **1973**, *A29*, 362.

Table I. Coordination Geometries and Resultant NMR Spin Systems for Seven-Coordinate $ML_5L'_2$ Complexes

structure[a]	hydrogen positns[a]	descript title (B&D no.)[b]	^{31}P and ^1H spectra[c]	coord plane occupatn	$^{31}P\{^1H\}$ spectrum[d]
1	4,5	planar heptagon	ABB′CC′XX	{0:7:0}	ABB′CC
	2,7		ABB′CC′XX′		ABB′CC′
	3,6		ABB′CC′XX′		ABB′CC′
2	1,2	hexagonal pyramid	ABB′CC′XX′	{1:6:0}	ABB′CC′
	1,3	(25)	ABCDD′XX′		$ABCD_2$
	1,4		ABB′C″B‴XX′		AB_4
3	5,6	pentagonal bipyramid	$AB_2CC'XX'$	{1:5:1}	AB_2C_2
	5,7	(5)	$AB_2CC'XX'$		AB_2C_2
	1,2		A_5X_2		A_5
4	2,3	capped trigonal	ABCDD′XX′	{1:3:3}	$ABCD_2$
	6,7	prism (of C_{3v} symmetry) (32)	ABCDD′XX′		$ABCD_2$
5	6,7	capped octahedral	ABCDD′XX′	{1:3:3}	$ABCD_2$
6	4,5	type structures	ABCDD′XX′		$ABCD_2$
7		(4) (1) (29)			
8	6,7	bicapped trigonal	$AB_2CC'XX'$	{1:2:2:2}	AB_2C_2
	3,4	bipyramid—C_{2v}	$AB_2CC'XX'$		AB_2C_2
	1,2	symmetry (2)	$ABB'CC'X_2$		ABB′CC′
9	1,2	bicapped square	ABB′B″B‴XX′	{1:2:4}	AB_4
	5,6	pyramid—C_{2v}	ABB′CC′XX′		ABB′CC′
	4,6	symmetry (10)	ABB′CC′XX′		ABB′CC′
	4,5		ABCDD′XX′		
10	6,7	capped trigonal	ABB′B′B″XX′	{1:4:2}	AB_4
11	4,5	prism—C_{2v}	ABB′CC′XX′		ABB′CC′
12	2,5	symmetry	ABCDD′XX′		$ABCD_2$
	2,4	(23) (16) (34)	ABB′CC′XX′		ABB′CC′

[a] In Figure 3. [b] Reference 9. [c] For the hydride-coupled ^{31}P and phosphorus-coupled hydride NMR spectra. [d] For the $^{31}P\{^1H\}$ NMR spectra.

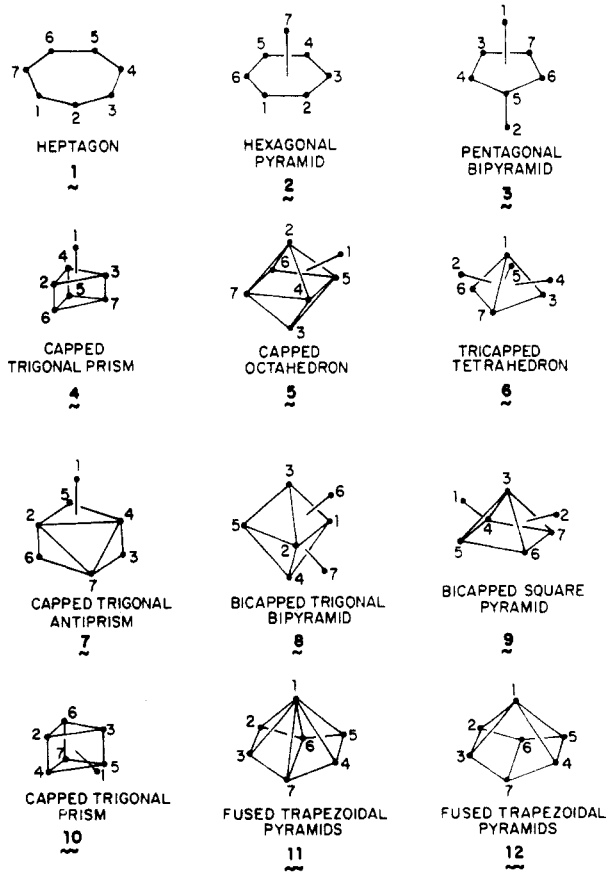

Figure 3. Structures and labeling of the heptagon and the 11 nonisomorphic convex polyhedra with seven vertices that have C_{2v} or higher symmetry.

stereochemistry. A descriptive title is given for each polyhedron together with the appropriate identification number from Britton and Dunitz.[9] In addition, the structures are characterized by the number of atoms in each plane perpendicular to the axis of highest symmetry (e.g., pentagonal bipyramid ≡ {1:5:1}). The 11 polyhedra are depicted in Figure 3. For completeness, the planar D_{7h} heptagon has also been included. In each case, we consider all possible structures in which the two hydrogen atoms are chemically equivalent and inquire what the coupled ^{31}P and ^1H, and decoupled $^{31}P\{^1H\}$ nuclear spin systems would be for that structure.

From a molecular structure point of view, structures **5**, **6**, and **7** are very closely related. They have been numbered in a similar fashion and, of course, give rise to the same spin systems. The same is true for structures **10**, **11**, and **12**.

The analysis of possible structures reveals that, for a system of two hydrogen and five phosphorus ligands, only two of the polyhedra give $AB_2CC'XX'$ and AB_2C_2 spin systems. These are the pentagonal bipyramid **3**, and the bicapped trigonal bipyramid of symmetry C_{2v} **8**, each of which gives rise to two isomers.

In point of fact, the situation is even simpler than this since the structures based on **8** are precisely those which arise from **3** when the distortions resulting from the inequalities of the ligands are taken into account. There are, therefore, two structural possibilities, **13** and **14**. Both are based on reasonable distortions of the pentagonal-bipyramid **3** and cannot be distinguished simply on the basis of the nature of their NMR spin systems.

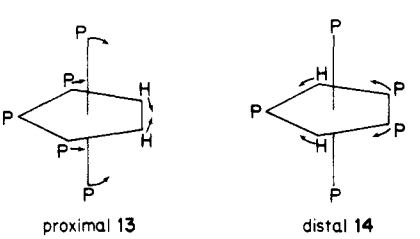

In octahedral chromium complexes, the two-bond P–P coupling constants conform to the relationship $|J(\text{cis})| > |J(\textit{trans})|$, with the signs of these two parameters being the same.[10] The magnitude of J_{AC} suggests that the angle

P_A–Cr–P_C deviates substantially from 90°, though this parameter relationship may be modified by seven-coordination. While in our preliminary report,[1b] we tentatively assigned the *proximal* stereochemistry to this complex, recent reports have led us to reconsider this assignment.

Although an X-ray crystal structure is not yet available for the title compound, structural and NMR data have appeared for two closely related compounds, $W(H_2)(CO)_3[P(i\text{-}Pr)_3]_2$, B,[2i] and $MoH_2[P(Me)_3]_5$, C.[2f] If the hydrogen atoms are considered to be simple monodentate ligands, the solid-state geometries of B and C are distorted pentagonal bipyramidal, with the hydrogens in the pentagonal plane. The tungsten compound B has the proximal structure **13** while the molybdenum compound C has the distal structure **14**. The two proximal hydrogens of B are best described as a single η^2-coordinated dihydrogen molecule on the basis of a very large H–H spin–spin coupling constant and a short H–H distance, as determined by neutron diffraction.[2i] The normal H–H coupling constant observed in our chromium complex A is consistent with the distal structure observed in the Mo complex C. We therefore assign a distal structure to A. In discussions in the rest of the paper, the structure and labeling in Figure 2 will be assumed.

Mechanistic Analysis: The Basic Permutation Sets. NMR line-shape changes resulting from exchange are analyzed by using a "jump model". The analysis can give information regarding the nuclear permutations that relate an initially labeled configuration to the (labeled) configuration after rearrangement. Such a model provides no *direct* mechanistic information regarding the actual reaction coordinate for rearrangement. All physical pathways leading to the correct permutational change are equally acceptable. Other physicochemical evidence must be considered to choose among the possibilities. In this section we outline the basic permutational sets that are distinguishable by the NMR method. In the sections that follow, we shall discuss the permutational sets that best simulate the experimental spectra and consider possible chemically reasonable physical pathways that correspond to the chosen sets.

For a "labeled" $CrH_2[P(OCH_3)_3]_5$ molecule, the permutations that generate all other possible labeled $CrH_2[P(OCH_3)_3]_5$ molecules comprise a group of order 5! × 2! = 240, i.e., the product of all permutations of the phosphorus nuclei among themselves and all permutations of the hydrogens among themselves. These 240 configurations include many arrangements related by the symmetry operations of the point group of the molecule (C_{2v}). With the numbering in Figure 2, the cyclic representations of the symmetry operations for this molecule are

$$E \quad \begin{matrix}1&2&3&4&5&6&7\\1&2&3&4&5&6&7\end{matrix} = (1)(2)(3)(4)(5)(6)(7)$$

$$C_2 \quad \begin{matrix}1&2&3&4&5&6&7\\1&3&2&5&4&7&6\end{matrix} = (1)(23)(45)(67)$$

$$\sigma_v \quad \begin{matrix}1&2&3&4&5&6&7\\1&2&3&5&4&7&6\end{matrix} = (1)(2)(3)(45)(67)$$

$$\sigma_{v'} \quad \begin{matrix}1&2&3&4&5&6&7\\1&3&2&4&5&6&7\end{matrix} = (1)(23)(4)(5)(6)(7)$$

There are, therefore, 240/4 = 60 unique Hamiltonians for the spin system. (Only permutations that exchange different spin Hamiltonians affect NMR line shapes.)

Table II. Relationship between the Basic Permutational Sets for the AB_2C_2 Phosphorus Spin System and the $AB_2CC'XX'$ Phosphorus-Proton Spin System for $CrH_2[P(OCH_3)_3]_5$

basic set for phosphorus atoms	corresponding set(s) for the full group	
I	1: (1534) (1425) (1435) (1524)	2: (15)(24) (14)(35) (14)(25) (15)(34)
II	3: (134)(25) (125)(34) (124)(35) (135)(24) (152)(34) (143)(25) (153)(24) (142)(35)	
III	4: (145) (154)	5: (14) (15)
IV	6: (1254) (1345) (1354) (1245) (1543) (1453) (1542) (1452)	7: (125) (134) (135) (124) (152) (143) (153) (142)
V	8: (25)(34) (24)(35)	
IV	9: (12)(345) (12)(354) (13)(245) (13)(254)	10: (12)(34) (12)(35) (13)(24) (13)(25)
VII	11: (254) (345) (245) (354)	12: (25) (34) (24) (35)
VIII	13: (123) (132)	14: (123)(45) (132)(45)
E	15: E	16: (45)

The methods employed for generation of the basic permutational sets have been described elsewhere.[11] This analysis yields 16 basic sets of permutations for the group 5! × 2!, including the set of symmetry operations of the C_{2v} point group. These are labeled 1–16; this numbering is also used to label the experimentally distinguishable types of line-shape behavior based on the jump model. In the exchange calculations, the exchange rates are defined as the rates at which one configuration is transformed to any other. A member of each basic set, with the corresponding label, is included in Table II. The remaining equivalent sets may be generated by applying the C_2, δ_v, and σ_v operations. There are, therefore, four equivalent sets of permutations within each basic set. Any one of these sets or any linear combination of them will give rise to the same calculated line shapes. In this way, all 240 elements of the molecular permutation group can be classified.

The $^{31}P\{^1H\}$ NMR spectrum of $CrH_2[P(OCH_3)_3]_5$ corresponds to an AB_2C_2 spin system, and the permutational subgroup is of order 5! = 120. There are 30 unique Hamiltonians and eight basic permutational sets, labeled I–VIII (Table II), which effect Hamiltonian exchange. For convenience in discussing the possible physical pathways for the exchange, the basic permutational sets for the AB_2C_2 phosphorus spin system, including all equivalent sets, are listed in Table III.

(10) (a) Ogilvie, F.; Clark, R. J.; Verkade, J. D. *Inorg. Chem.* **1969**, *8*, 1904. (b) Moser, E.; Fischer, E. O. *J. Organomet. Chem.* **1968**, *15*, 157. (c) Bertrand, R. D.; Ogilvie, F. B.; Verkade, J. D. *J. Am. Chem. Soc.* **1970**, *92*, 1908. (d) Ogilvie, F. B.; Jenkins, J. M.; Verkade, J. G. *Ibid.* **1970**, *96*, 1916.

(11) Jesson, J. P.; Meakin, P. *Acc. Chem. Res.* **1973**, *6*, 269.

Table III. Basic Permutational Sets for the AB_2C_2 Phosphorus Spin System in $CrH_2[P(OCH_3)_3]_5$

	ϵ	C_2	σ_v	σ_v'
I	(15)(24)	(14325)	(15)(243)	(1425)
	(14)(35)	(53412)	(14)(235)	(1534)
	(15)(34)	(43521)	(15)(234)	(1435)
	(14)(25)	(54213)	(14)(253)	(1524)
II	(25413)	(125)(34)		
	(12534)	(134)(25)		
	(12435)	(135)(24)		
	(13524)	(124)(35)		
	(15243)	(152)(34)		
	(14352)	(143)(25)		
	(15342)	(153)(24)		
	(45123)	(142)(35)		
III	(15)(23)	(145)	(15)	(145)(23)
	(14)(23)	(154)	(14)	(154)(23)
IV	(1325)	(1245)	(125)	(13245)
	(1234)	(1354)	(134)	(12354)
	(1235)	(1345)	(135)	(12345)
	(1324)	(1254)	(124)	(13254)
	(1523)	(1542)	(152)	(15423)
	(1432)	(1453)	(143)	(14532)
	(1532)	(1543)	(153)	(15432)
	(1423)	(1452)	(142)	(14523)
V	(25)(34)	(2534)		
	(24)(35)	(2435)		
VI	(13)(25)	(12453)	(1253)	(13)(245)
	(12)(34)	(13542)	(1342)	(12)(354)
	(12)(35)	(13452)	(1352)	(12)(345)
	(13)(24)	(12543)	(1243)	(13)(254)
VII	(25)	(2453)	(253)	(245)
	(34)	(2354)	(234)	(354)
	(35)	(2345)	(234)	(345)
	(24)	(2543)	(243)	(254)
VIII	(13)(45)	(123)	(123)(45)	(13)
	(12)(45)	(132)	(132)(45)	(12)
E	(23)(45)	(1)(2)(3)(4)(5)	(45)	(23)

Table II is arranged to clarify the correspondences between the subgroup (I–VIII) and the full group (1–16). For each basic permutational set, the equivalent basic set is displayed that corresponds to the simplest phosphorus nuclear exchange. This has been done for clarity and should not be taken to imply a preference for a particular set. Those sets that include hydrogen atom exchange are simply related to those which appear in Table II. Consider the phosphorus exchange mechanism I and the corresponding members of the full group, mechanisms 1 and 2. Since the permutation (1534) appears in a basic set for mechanism 1, the permutation (1534)(67) will appear in one of the basic sets for mechanism 2. For the mechanisms 3 and 8, permutations related as outlined above will appear in different equivalent basic sets for the same mechanism.

Line-Shape Calculations. The density matrix approach employed in the line-shape calculations has been disclosed in detail elsewhere.[11] For the five-spin system appropriate to the $^{31}P\{^1H\}$ spectrum, the Liouville space is of dimension 1024 × 1024. This may be factored under weak radio-frequency field conditions into five subspaces, the largest of which has dimension 100 × 100 corresponding to the $I_z = -^1/_2 \rightarrow {}^1/_2$ transitions. Factoring because of point-group symmetry and magnetic equivalance reduced the order of the largest complex non-Hermitian matrix to 34. The matrices could be diagonalized directly, and no approximations were necessary for the $P^{31}\{^1H\}$ spectral simulations.

The seven-spin system necessary for simulation of the ^1H spectrum generates a Liouville space of order 16384. The $I_z = -^1/_2 \rightarrow {}^1/_2$ transitions correspond to a submatrix of dimension 1225 × 1225. When X factoring is introduced, the largest matrices are of dimensions 400 × 400 for the phosphorus transitions and 200 × 200 for the hydrogen transitions. Point-group symmetry factoring and magnetic equivalence factoring reduce the largest matrix for the hydrogen transitions to dimension 64 × 64. This is just within the capabilities of our current system of programs (largest matrix, 70 × 70 on a DEC 10 computer system). However, the long running time for one calculation (29 min) and the projected cost of simulating all the mechanisms led us to examine the line omission approximation[12] for this system. Simulations obtained from calculations in which lines of intensity $<10^{-4}$ were omitted were found to be visually indistinguishable from those derived from complete calculations. All simulations of the ^1H spectra were carried out by using a line omission thereshold of 10^{-5}. We suspect that this situation may arise from the fact that the energy calculation uses simple product spin functions rather than symmetry-adapted spin functions. Accumulation of round-off errors in the transformation of the intensities can lead to extremely small, nonzero intensities, which should be identically zero.

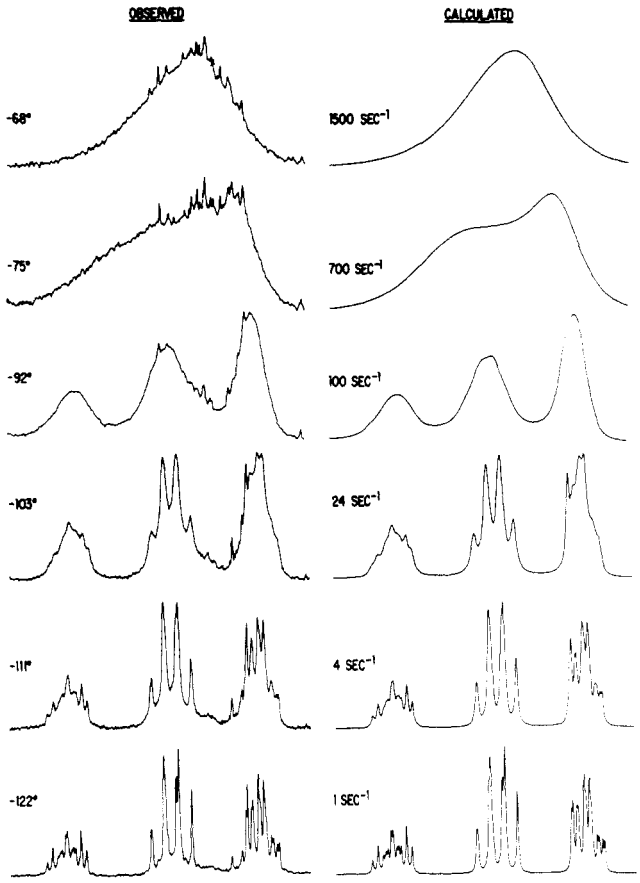

Figure 4. $^{31}P\{^1H\}$ (36.43-MHz) NMR spectra for $CrH_2[P(OCH_3)_3]_5$ over a range of temperature together with simulated spectra for the basic permutational set VI.

Mechanism. Permutation Distinctions. (1) $^{31}P\{^1H\}$ Spectra. The first column of Figure 4 shows the observed $^{31}P\{^1H\}$ spectrum of $CrH_2[P(OCH_3)_3]_5$ as a function of temperature. The spectral parameters given in section B were used to calculate the line-shape behavior for each of the basic permutational sets I–VIII outlined in section E. These results are displayed in Figures 5 and 6 that are arranged such that a given row corresponds to the same *effective* rate of rearrangement, i.e., the product of the rate constant and the number of permutations in the basic set, for each of the different mechanisms.

Four permutational mechanisms fail to average the phosphorus environments (Figure 5). The high-tempera-

(12) Meakin, P.; Jesson, J. P. *J. Am. Chem. Soc.* **1973**, *95*, 7272.

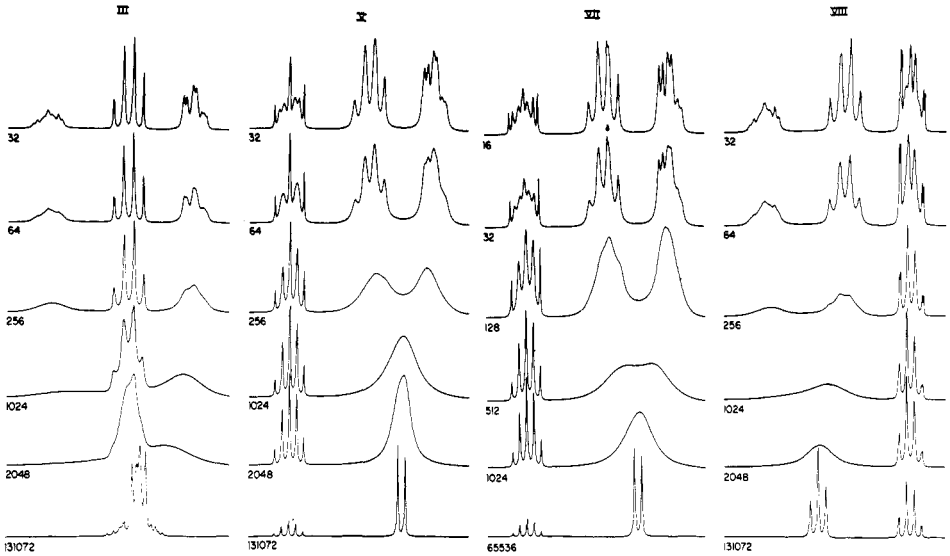

Figure 5. Calculated $^{31}P\{^1H\}$ (36.43-MHz) line shapes as a function of exchange rate for phosphorus exchange mechanisms III, V, VII, and VIII. The exchange rates are in units of inverse seconds.

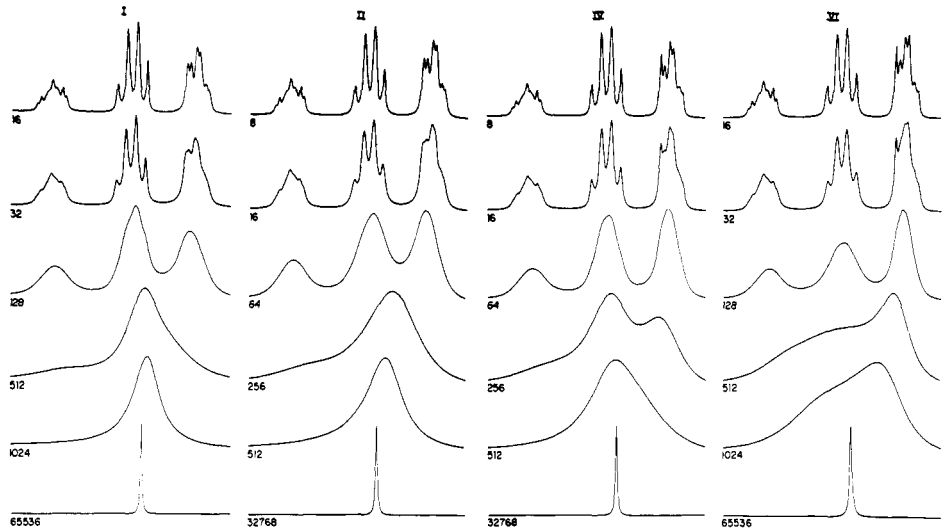

Figure 6. Calculated $^{31}P\{^1H\}$ (36.43-MHz) line shapes as a function of exchange rate for phosphorus exchange mechanisms I, II, IV, and VI. The exchange rates are in units of inverse seconds.

ture limit for mechanisms V and VII is a nearly first-order AB_4 spectrum. Mechanism VIII leads to a nearly first-order A_3B_2 spectrum. The high-temperature limit for mechanism III is also an A_3B_2 spectrum, but the spectrum is quite complex since the effective $|J/\delta|$ is large. Clearly, these permutational mechanisms may be excluded from further consideration.

Mechanisms I, II, IV, and VI (Figure 6) all produce the correct spectrum in the limit of fast exchange. Cases I and II may be eliminated, since the simulations for exchange rates in the range 8–32 s^{-1} do not compare well with the experimental spectra. Mechanisms IV and VI, on the other hand, produce simulations quite similar to the experimental spectra at slower exchange rates. A distinction can be made, however, for exchange rates in the region 100–1000 s^{-1} on the basis of the intensity distributions in the exchange-broadened multiplets. Close comparison of the simulations with the experimental spectra shows clearly that VI is the permutational mechanism operative for $CrH_2[P(OCH_3)_3]_5$. The calculated spectra in Figure 4 were obtained by using mechanism VI; temperature dependences of the chemical shifts were taken into account. Attempts to match these spectra using mechanism IV resulted in substantially poorer agreement.

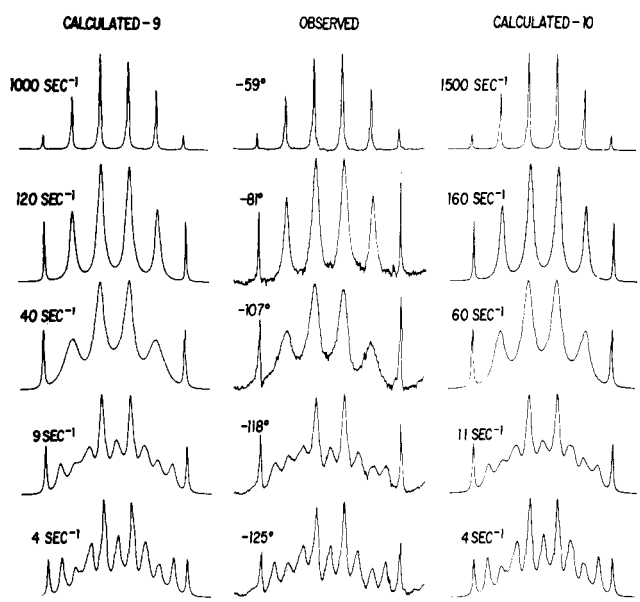

Figure 7. Observed and calculated 90-MHz ^1H hydride NMR spectra for $CrH_2[P(OCH_3)_3]_5$. The calculated spectra are for basic permutational sets 9 and 10 (Table I).

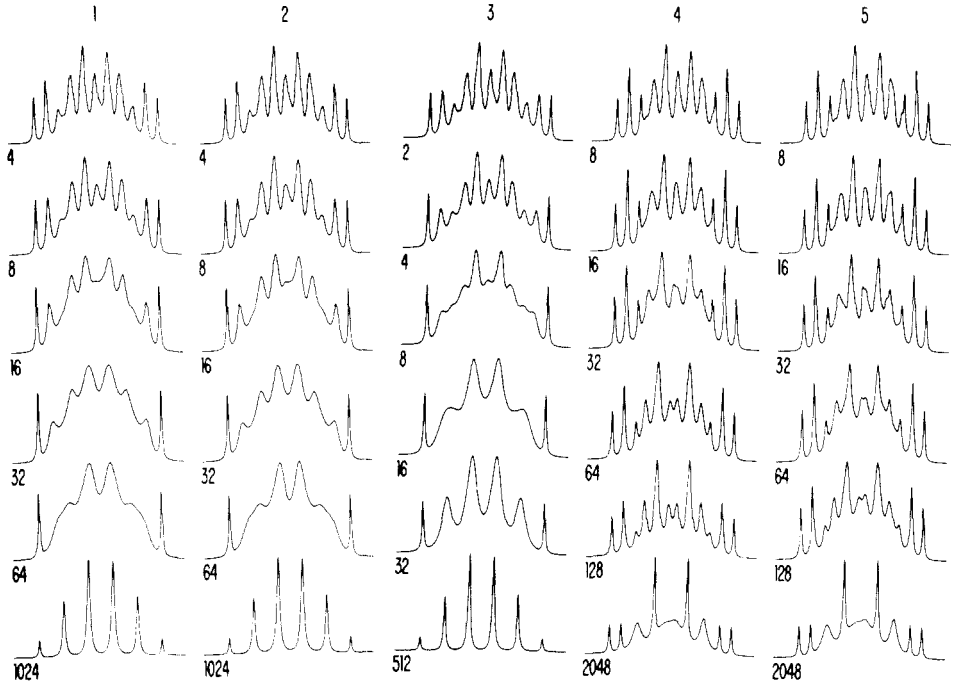

Figure 8. Calculated 90-MHz ^{1}H hydride NMR spectra for $CrH_2[P(OCH_3)_3]_5$ as a function of exchange rate for basic permutational sets 1-5 (Table I). Exchange rates are in units of inverse seconds.

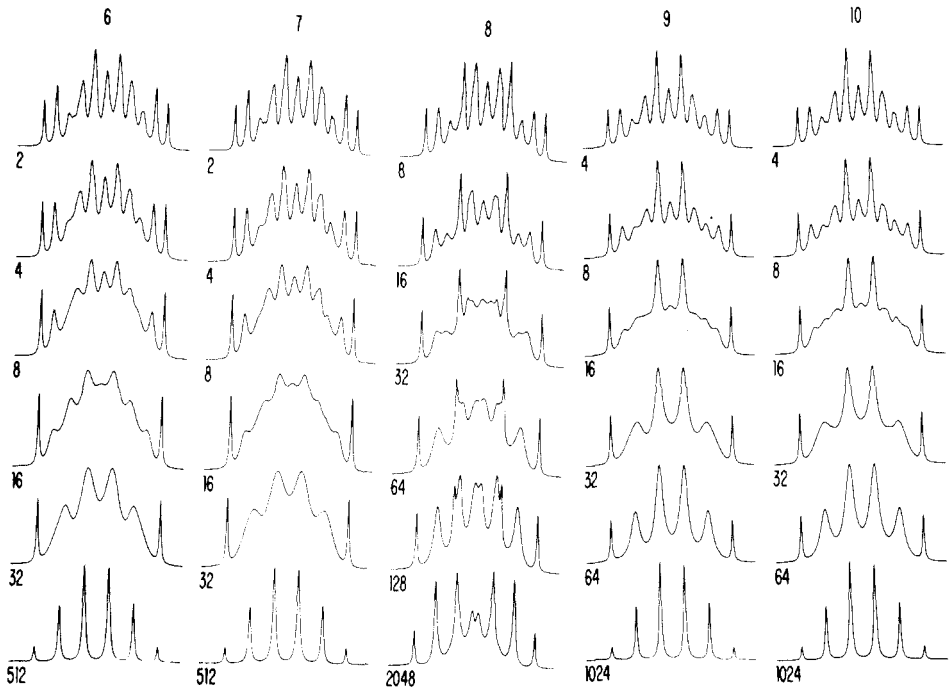

Figure 9. Calculated 90-MHz ^{1}H hydride NMR spectra for $CrH_2[P(OCH_3)_3]_5$ as a function of exchange rate for basic permutational sets 6-10 (Table I). Exchange rates are in units of inverse seconds.

(2) ^{1}H Spectra. The center column of Figure 7 shows the observed 90-MHz ^{1}H hydride spectrum of $CrH_2[P(OCH_3)_3]_5$. The two outer lines remain sharp at all temperatures. In terms of the quantum numbers of I_{z_H} and I_{z_P}, these correspond to the transitions $|-1,-5/2\rangle \rightarrow |0,-5/2\rangle$ and $|0,-5/2\rangle \rightarrow |1,-5/2\rangle$ for one of the lines and to the same functions with $I_{z_P} = +5/2$ for the two transitions corresponding to the other line. The absence of exchange effects for these transitions permits direct measurement of T_2 at each temperature. These T_2 values have been used in the spectral simulations.

Simulations of the ^{1}H spectra at various exchange rates for all mechanistic models are presented in Figures 8–10, using the spectral parameters of section B. As expected, only those mechanisms derived from the basic phosphorus exchange mechanisms I (1, 2), II (3), IV (6, 7), and VI (9, 10) lead to the correct high-temperature limit sextet. On this basis, the exchange mechanisms 4, 5, 8, and 11–16 are excluded. Cursory visual comparison of the remaining calculated spectra with experiment excludes mechanisms 1, 2, 6, and 7. We are, therefore, left with mechanisms 3, 9, and 10. Careful comparison of experiment and theory rules out mechanism 3. Thus, from the ^{1}H spectra alone we can narrow the choice to mechanism 9 or 10, the same basic permutational sets we would have predicted from the earlier considerations of the $^{31}P\{^1H\}$ spectra (Table I); mechanisms 9 and 10 correspond to phosphorus exchange VI. The simulations (Figure 9) indicate that mechanisms

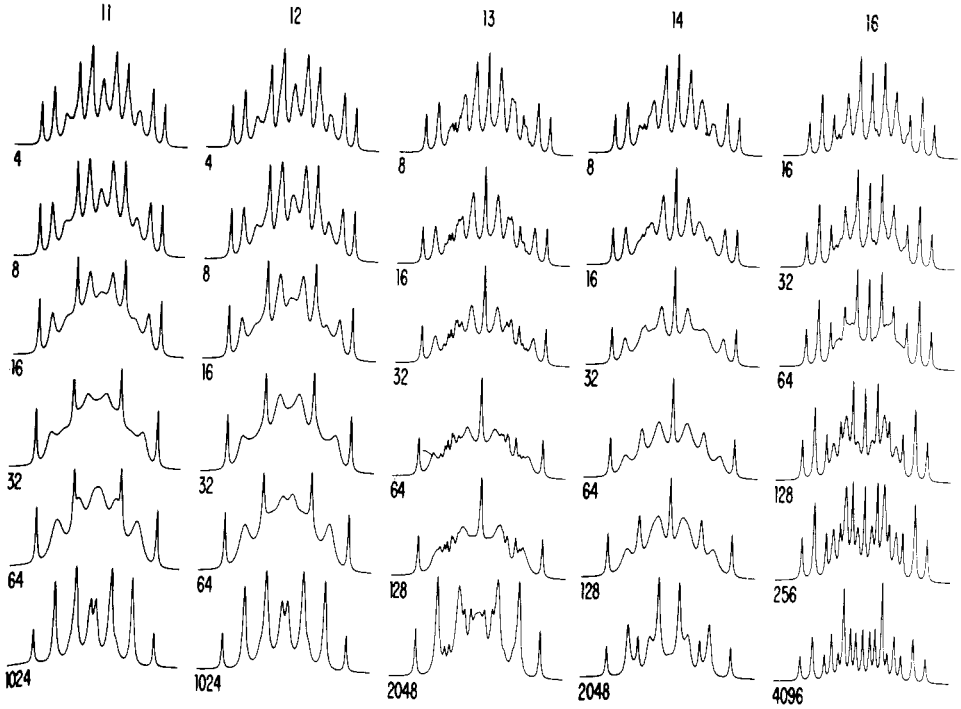

Figure 10. Calculated 90-MHz ^1H hydride NMR spectra for $CrH_2[P(OCH_3)_3]_5$ as a function of exchange rate for basic permutational sets 11–16 (Table I). The exchange rates are in units of inverse seconds.

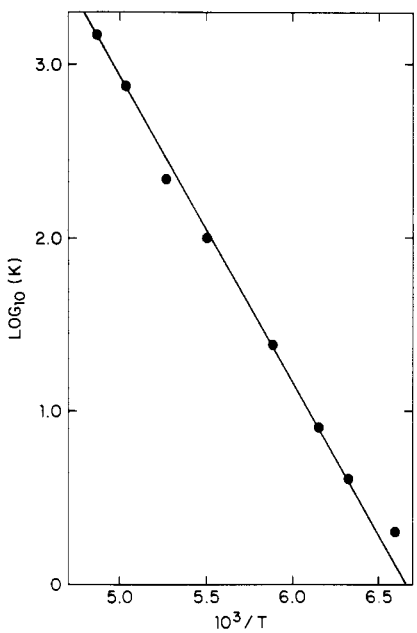

Figure 11. Arrhenius plot for $^{31}P\{^1H\}$ data for $CrH_2[P(OCH_3)_3]_5$.

9 and 10 lead to rather similar spectra. At the same time, uncertainties in some of the spectral parameters preclude a clear choice, based on the best matches displayed in Figure 7. We will, therefore, consider both possibilities in our discussion of physical models (vide infra).

Exchange rates for the $^{31}P\{^1H\}$ spectra are presented in Figure 11 as an Arrhenius plot. The straight line corresponds to the rate expression

$$k(T) = 10^{11.7}e^{-8100/RT}$$

Alternatively, the temperature dependence of the rate can be expressed in terms of the Eyring equation

$$k(T) = K(kT/h)e^{-G^*/RT}$$

and the activation parameters are $\Delta G^*(298) = 9400$ cal mol^{-1}, $\Delta G^*(179) = 8700$ cal mol^{-1}, $\Delta H^* = 7650$ cal mol^{-1}, and $\Delta S^* = -5.9$ cal mol^{-1} deg^{-1}, assuming the transmission coefficient $K = 1$.

Table IV. Basic Permutational Sets for $CrH_2[P(OCH_3)_3]_5$: Mechanisms 9 and 10

	A (E)	B (C_2)	C (σ_v)	D (σ_v')
9	(13)(25)(67)	(13542)	(13)(254)	(1352)(67)
	(13)(24)(67)	(13452)	(13)(245)	(1342)(67)
	(12)(35)(67)	(124)(53)	(12)(345)	(1253)(67)
	(12)(34)(67)	(12543)	(12)(354)	(1243)(67)
10	(13)(25)	(13542)(67)	(13)(254)(67)	(1352)
	(13)(24)	(13452)(67)	(13)(245)(67)	(1342)
	(12)(35)	(12453)(67)	(12)(345)(67)	(1253)
	(12)(34)	(12543)(67)	(12)(354)(67)	(1243)

Mechanism. Physical Models. We now consider the possibilities for physical mechanisms based on the permutations 9 and 10. There are four equivalent sets of permutations for each; e.g., 9A = (13)(25)(67), 9B = (13542), 9C = (13)(254), 9D = (1352)(67), etc., with the sets of permutations related by the operations of the point group as previously described (Table IV). We have constructed reaction pathways for the eight possibilities based on a quasi-least-motion formalism described in the Appendix. While we expected to generate eight different transition-state models, we find, within this modeling technique, that only four of them are distinct (Figure 12). The A and B sets for a given mechanism led to essentially the same intermediate structure, as do the C and D sets. Examination of the possible transition-state geometries determined in this way leads to a preferred reaction pathway.

1. Figure 12a shows the hypothetical transition state derived from pathways 10A and 10B. The hydride ligands are nearly coincident, and three of the phosphorus ligands sharing a plane have P–Cr–P angles of 48°. In addition, the five phosphorus ligands approach an unrealistic degree of coplanarity. Given that the Tolman cone angle[13] defined for the trimethyl phosphite ligand is 107°, we anticipate that this pathway would have a activation energy substantially higher than the ~8 kcal/mol that we find.

(13) Tolman, C. A. *Chem. Rev.* **1977**, *77*, 313.

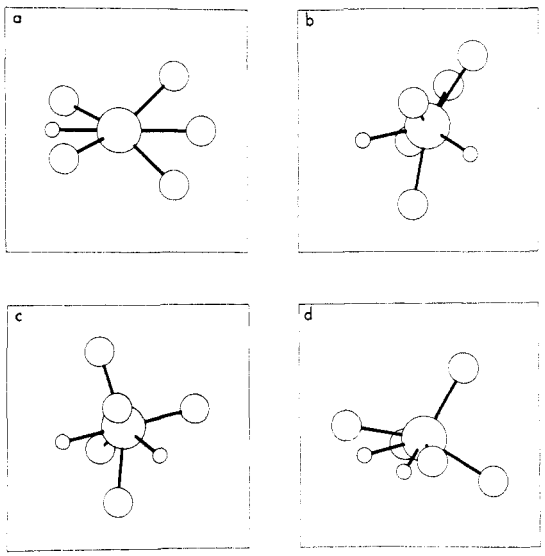

Figure 12. Transition state models derived for *distal*-$CrH_2[P(OCH_3)_3]_5$: (a) mechanism 9A or 9B; (b) mechanism 10A or 10B; (c) mechanism 10C or 10D; (d) mechanism 9C or 9D.

2. The transition state derived from pathways 9A and 9B is shown in Figure 12b. The geometry approximates that of a bicapped square pyramid (**9** in Figure 3), with the hydride ligands forming part of the base. While the hydride placement is now much more favorable than in the corresponding representation of mechanism 10, the steric environment of the phosphorus ligands is essentially the same. Hence we expect that the energetics of this pathway will also be inconsistent with the experimentally determined value.

3. Figure 12c is the transition state derived from pathways 10c and 10d. The geometry corresponds rather closely to a capped octahedron (**5** in Figure 3) with no apparent steric crowding, even when contact radii are used. We believe that the actual physical pathway for the rearrangement is best described by one or both of these mechanisms.

4. Pathways 9C and 9D led to the transition state in Figure 12d. The CrP_5 fragment approximates an octahedral complex with one vacant site. The hydride positions may be described as insertion of H2 into a basal edge of a square pyramid. Alternatively, the structure can be viewed as a highly distorted fuzed trapezoidal pyramid (**11** and **12** in Figure 3). There is no obvious steric crowding in this structure as drawn. However, drawings made employing van der Waals' contact radii for the atoms show that each hydride ligand is in fact inside the contact sphere of its neighboring phosphorus atom. Such an arrangement seems unlikely if other, more favorable pathways are available.

Figure 13 shows a series of "snapshots" for Mechanism 10D, based on the permutation (1253). The rearrangement pathway can be described most simply in terms of a trigonal bipyramid with the hydride ligands on different equatorial edges. In this description, rearrangement occurs by the motion of a single hydride to an axial–equatorial edge, accompanied by appropriate relaxation of the heavy-atom framework (eq 1). The process may be vis-

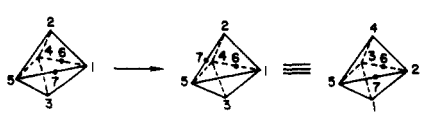

overall exchange: (1243) (1)

ualized as a Berry pseudorotation of the trigonal bipyramid

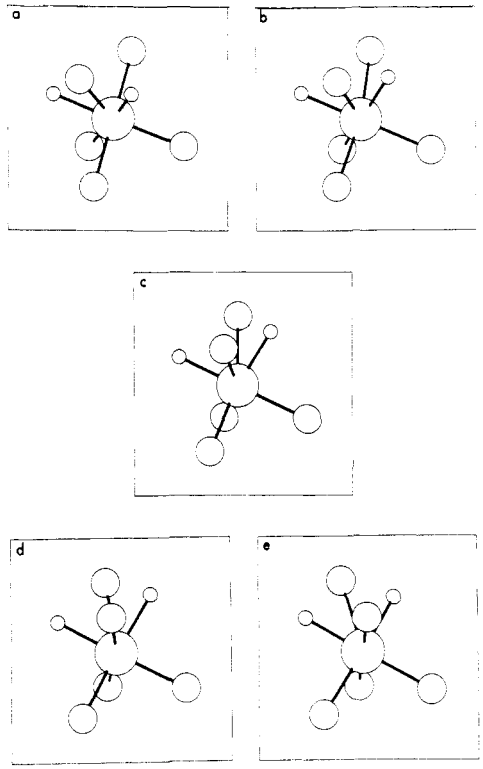

Figure 13. "Snapshots" of *distal*-$CrH_2[P(OCH_3)_3]_5$ undergoing the permutation (1253) at (a) 0%, (b) 25%, (c) 50%, (d) 75%, and (e) 100% rearrangement.

formed by the five phosphorus ligands, with the hydride ligands moving to the new equatorial edges.

We can account for the identity of the two descriptions (10C and 10D) of the rearrangement in terms of the physical motion described. If we apply the permutation (13)(245)(67) and follow it by a C_2 operation, we find that the resulting arrangement of ligands is exactly that resulting from the permutation (1342) (eq 2). Thus, the two,

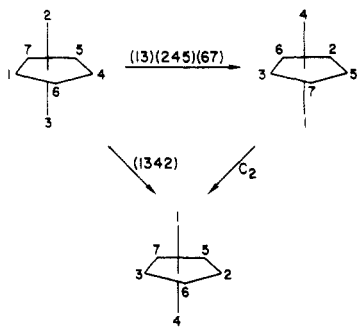

(2)

nominally distinct, sets of permutations give the same results. The effect of the hydride permutation in the representation 10C is nullified by the shift of the 4,5 ligands.

Conclusions

The possible mechanistic pathways for exchange in $CrH_2[P(OCH_3)_3]_5$ have been considered in terms of the favored equilibrium geometry, the permutational nature of the exchange, seven-coordinate polyhedra of C_{2v} symmetry and higher, and concepts of least motion.

We have shown that there are 16 possible basic permutational sets, only two of which give the correct simulated line-shape behavior with temperature. The two sets correspond to identical permutational behavior of the phosphorous ligands and differ only in the question of whether or not the two hydride ligands permute. The

possibility involving no hydride permutation gave a slightly better fit to the data and was, therefore, marginally preferred.

The physical mechanisms that correspond to the experimentally established permutations considered were examined by employing a quasi-least-motion simulation. We have concluded that the most probable mechanism involves a simultaneous exchange of the two axial phosphorus ligands with two of the equatorial phosphorus ligands. The hydride ligands simply move to the new equatorial edges. In the (distorted) distal pentagonal-bipyramidal structure that is favored as the equilibrium geometry, this corresponds to permutation of the CrP_5 framework via a "Berry pseudorotation" type process.

Line-shape analysis in a seven-spin system is a complex problem; the NMR line-shape study of $CrH_2[P(OCH_3)_3]_5$ described in this paper involves an analysis of the most complex spin system yet treated in detail and further illustrates the power of a systematic analysis of the basic permutations to clarify and eliminate mechanistic possibilities.

Acknowledgment. We wish to acknowledge the fine technical assistance of M. A. Cushing, Jr., G. Watunya, and F. N. Schock.

Appendix

In order to facilitate the visualization of dynamical processes such as mutual exchange in coordination complexes, electrocyclic reactions, and intramolecular Diels–Alder reactions, we have developed a methodology for mapping an initial atomic configuration into a final one. The first step is to assure maximum coincidence of the (labeled) atoms in the initial and final arrangements. This is accomplished by requiring that the mass-weighted residual be at a minimum

$$m^i[R^i(\text{final}) - R^i(\text{initial})]^2$$

where the R^i's are particle position vectors. It is generally convenient to operate in a center-of-mass coordinate system, though with simple coordination complexes it may be acceptable to place the origin at the central atom. The second step involves motion along some pathway leading from the initial to the final configuration. Least-motion pathways defined in Cartesian coordinates are generally unsuitable, giving physically unreasonable intermediate structures. *Quasi-least-motion* pathways may be mapped, either in spherical polar coordinates (suitable for simple coordination complexes) or in internal coordinates (the most general case). While these pathways will not in general correspond to the lowest energy route from starting material to products, they should represent qualitative approximations of the actual pathways.

We have used the spherical polar model for the rearrangement mechanisms for the distal isomer of $CrH_2[P(OCH_3)_3]_5$. The trimethyl phosphite ligands were replaced by points of equal mass displaced outward along the Cr–P bond direction to the center-of-mass for the phosphite group.

Registry No. $Cr[P(OMe)_3]_5H_2$, 92842-95-0; $Cr[P(OMe)_3]_6$, 70948-62-8.

Trinuclear Clusters of Early Transition Metals: Jahn–Teller Distortions and Electronic Structure†

Yuansheng Jiang* (Yuan-sun Kiang) and Aoqing Tang

Institute of Theoretical Chemistry, Jilin University, Changchun, Peoples Republic of China

Roald Hoffmann*

Department of Chemistry, Cornell University, Ithaca, New York 14853

Jinling Huang* and Jiaxi Lu

Fujian Institute of Research on the Structure of Matter, Academia Sinica, Fuzhou, Peoples Republic of China

Received April 18, 1984

A detailed theoretical study of a trinuclear eight-electron cluster with a distorted metal core, $Mo_3S_2Cl_9^{3-}$, leads to some general conclusions about the role of different capping, bridging, and terminal ligands in determining the electronic and geometrical structure of trinuclear clusters of the early transition metals.

The early transition-metal cluster compounds are distinguished from similar clusters involving 8B elements by the typically high oxidation state of the metal component and by halogens or other electronegative atoms as ligands. A variety of oxidation states or electron counts exists. During the past few years, much research has been carried out on and much attention has been paid to the trinuclear metal cluster systems, one of the representative species of experimental and theoretical importance.[1] Dozens of complexes of this type have been prepared and structurally characterized.[2-43] At the same time, theoretical investigations were also developing.[44-49]

†Dedicated to the memory of our friend and colleague Earl Muetterties.

(1) Müller, A.; Jostes, R.; Cotton, F. A. *Angew. Chem., Int. Ed. Engl.* **1980**, *19*, 875.
(2) Cotton, F. A.; Mague, J. T. *Inorg. Chem.* **1965**, *3*, 1402.
(3) Goldberg, S. Z.; Spinack, B.; Stanley, G.; Eisenberg, R.; Braitsch, D. M.; Muller, J. S.; Abkowitz, M. *J. Am. Chem. Soc.* **1977**, *99*, 110.
(4) King, R. B.; Braitsch, D. M.; Kapoor, P. N. *J. Am. Chem. Soc.* **1975**, *97*, 60.
(5) Fisher, E. O.; Rohrscheid, F. *J. Organomet. Chem.* **1966**, *6*, 53.
(6) Churchill, M. R.; Chang, S. W. Y. *J. Chem. Soc., Chem. Commun.* **1974**, 248.
(7) Müller, A.; Ruck, A.; Dartmann, M.; Reinsch-Vogell, U. *Angew. Chem., Int. Ed. Engl.* **1981**, *20*, 483.

0276-7333/85/2304-0027$01.50/0